THE ASTRONOMICAL JOURNAL VOLUME 107, NUMBER 3 MARCH 1994

SELF-GRAVITATING POLAR RINGS IN AXISYMMETRIC AND TRIAXIAL GALAXY POTENTIALS

MAGDA ARNABOLDI

Mt. Stromlo and Siding Spring Observatories, Australian National University, ACT 2611, Australia and International School for Advanced Studies, S.I.S.S.A., Via Beirut 2, Trieste, I 34014, Italy
Electronic mail: magda@merlin.anu.edu.au

LINDA S. SPARKE

Washburn Observatory, University of Wisconsin-Madison, 475 N. Charter Street, Madison, Wisconsin 53706
Electronic mail: sparke@madraf.astro.wisc.edu

Received 1993 August 20; revised 1993 November 9

ABSTRACT

A number of early type galaxies show a polar ring of gas, dust, and stars lying roughly perpendicular to the apparent major axis of the central galaxy. Here, we study the dynamics of a self-gravitating annulus of matter which is inclined to the principal planes of a triaxial galactic potential tumbling about its short axis. In a steadily precessing equilibrium state, the precession rate of the ring in the potential must be equal to the tumbling speed of the triaxial figure. As in an oblate galaxy, both stable and unstable equilibria exist: in the tumbling triaxial potential, there are stable equilibria bending toward the equator, if the ring is light, and toward the pole, at higher ring mass. The former are similar to the "anomalous retrograde orbits," while the latter resemble the stable equilibria for a self-gravitating ring in an oblate potential. We follow the time evolution of unstable polar rings. In an oblate galaxy potential, even if the ring is not sufficiently massive to be stabilized, self-gravity can still cause the characteristic warp up toward the pole. In the triaxial potential, when the inclination of the polar ring is not such that its precession rate matches the galaxy tumbling speed, the ring can wobble gently in a quasiperiodic manner if it is massive enough, but is disrupted if its mass is too low.

1. INTRODUCTION

Polar rings (PR) around early type galaxies consist of rings of gas, dust, and stars, roughly aligned with the galaxy minor axis; the "Spindle," NGC 2685, is the most famous example. The peculiar orientation of the ring was formerly thought to suggest an intrinsic prolate shape for the central galaxy, but Schechter & Gunn (1978) showed that stars in the central galaxy of NGC 2685 were rotating in a direction nearly orthogonal to the ring, as expected for a disk galaxy seen edge-on. The Polar Ring Catalogue (PRC) of Whitmore *et al.* (1990) lists six "kinematically confirmed" rings in which the angular momentum of the ring material is known to be almost perpendicular to that of the central galaxy, and 100 further "good" or "possible" candidates. Analysis of this catalogue indicates that about 0.5% of S0 galaxies have PR; they are neither common nor extremely rare. The rings do not lie exactly perpendicular to the projected minor axes of the underlying galaxy, but are often misaligned by 20° or 30° (Whitmore 1991).

PR probably formed from material accreted from outside the system: e.g., by merger with a companion galaxy. Radio synthesis observations (Schechter *et al.* 1984; van Gorkom *et al.* 1987) show the rings to be rich in neutral hydrogen, often containing several billion solar masses of gas, while the central galaxy is gas poor. Some PR (e.g., NGC 4650A) are blue, suggesting recent star formation; others, such as UGC 7576 (Mould *et al.* 1982) are redder with little Hα emission or other sign of young stars. The central galaxy of the polar ring AM 2020−504 has an ultraviolet spectrum characteristic of a starburst (Arnaboldi *et al.* 1993b), perhaps indicating that gas has flowed into the galaxy from the ring.

It is somewhat surprising that PRs show a regular tilted structure, since the gravitational field of the flattened central elliptical or S0 galaxy has a quadrupole component, which causes the orbits of ring particles to precess about the pole at a rate which depends on the radius and orbital inclination. Simple estimates indicate that differential precession should destroy the flatness of a PR in much less than a Hubble time, and would imply that the observed structures have been formed only recently. But severely warped rings are not common, and many of them (e.g., UGC 7576; Schechter *et al.* 1984; Mould *et al.* 1982; NGC 5122; PRC) look quite smooth and have time to form the observed stars; this suggests that the rings have been stabilized in some way.

Whitmore (1991) divided objects in the PRC into two main morphological classes: "wide" and "narrow" rings. Rings around small S0 galaxies such as NGC 4650A extend up to several times the optical radius of the underlying galaxies, and appear as wide and nearly coplanar annuli with a hole around the central S0. The rotation curve of the ring gas has been measured in a number of these systems (Schweizer *et al.* 1983, hereafter referred to as SWR; Whitmore *et al.* 1987a, hereafter referred to as WMS); it is nearly flat, indicating a substantial dark halo. Detailed dynamical modeling has been used to constrain

 0004-6256/94/107(3)/958/13/$0.90

the three-dimensional shape of the halo (e.g., WMS; Sackett & Sparke 1990). The PRs encircling rounder central objects appear narrow and internal to the optical radius of the central galaxy. In the system AM 2020−504, the prototype of this class, the central galaxy is an E4 elliptical, with a fast-rotating decoupled core (Whitmore *et al.* 1987b; Arnaboldi *et al.* 1993a). The luminous narrow rings may be dynamically similar to the minor-axis dust lanes found in elliptical galaxies (Bertola 1987). In these objects, the intrinsic shape of the central galaxy may be triaxial rather than axisymmetric.

Sparke (1986) showed that self-gravitating PRs may have long-lived equilibrium states in the potential of an axisymmetric oblate galaxy. In this paper we consider the equilibria and time-dependent behavior of massive rings in a potential with triaxial symmetry, tumbling about its short axis. We briefly describe the equations of motions and the gravitational potential used to model the galaxy in Sec. 2. The equilibrium configurations and their stability are presented in Sec. 3; the evolution of massive rings in axisymmetric and triaxial potentials is discussed in Sec. 4, and Sec. 5 contains our conclusions.

2. EQUATIONS OF MOTION

In what follows, the mass distribution of the central galaxy is modeled as an oblate or triaxial ellipsoid. The orbit of any star or gas cloud in the PR then precesses about one of the principal axes of the galaxy; if precession is slow compared to the time required to complete one orbit, then the change in the orbital elements due to the galaxy's asphericity may be calculated by averaging over the rapid orbital motion. Further, the gravitational force exerted by that star on the rest of the material may be replaced by the force due to a torus of material spread over the orbit (e.g., Goldreich 1966). Because the galaxy is flattened, the actual orbits will be somewhat oval rather than circular, and stars will not move on them with precisely uniform speed. But these effects are first order in the galactic asphericity, and change the precession-inducing torques only at second order; we neglect them in this work. Thus a set of concentric circular massive wires, with spin angular momentum calculated from the spherically averaged gravitational field of the galaxy, serves as a model for the PR. Gravity is assumed to be the only force acting: ring particles feel both the gravitational influence of the central galaxy and torques induced by other ring material. Dissipative forces and radial mass flow are ignored.

Any one wire may be described by its radius r, which is constant since no dissipation occurs, by its mass m, the inclination $\theta(t)$ to the (x,y) principal plane of the galaxy, and the azimuth $\phi(t)$ at which the orbit cuts the plane in the ascending direction (toward $z>0$). Following the conventions of Goldstein (1980, Sec. *4.4*) and using ψ to label the position of a point along the orbit, the energy E is given by

$$E=\frac{mr^2}{4}(\dot\theta^2+\dot\phi^2\sin^2\theta)+\frac{mr^2}{2}(\dot\psi+\dot\phi\cos\theta)^2 + V(r,\theta,\phi), \tag{1}$$

where $V(r,\theta,\phi)$ is sum of the gravitational potential energy V_g of the wire in the field of the galaxy and the potential V_m due to the other ring material. The energy does not depend on the coordinate ψ, hence the conjugate momentum

$$p_\psi=mr^2(\dot\psi+\dot\phi\cos\theta) \tag{2}$$

is conserved; this is just the angular momentum of the orbital motion, $p_\psi=mr^2\Omega(r)$. The other two momenta are p_ϕ, the z angular momentum, and p_θ, the angular momentum about the instantaneous line of nodes where the ring cuts the plane $z=0$. The equations of motion for these are given by

$$p_\theta=\frac{mr^2}{2}\dot\theta,$$
$$\dot p_\theta=-\frac{\partial V(r,\theta,\phi)}{\partial\theta}-2\frac{(p_\phi-p_\psi\cos\theta)(p_\psi-p_\phi\cos\theta)}{mr^2\sin^3\theta}, \tag{3}$$

$$p_\phi=\frac{mr^2}{2}\dot\phi\sin^2\theta+p_\psi\cos\theta,$$
$$\dot p_\phi=-\frac{\partial V(r,\theta,\phi)}{\partial\phi}. \tag{4}$$

When the galactic potential tumbles steadily about the axis z at a rate Ω_p, it is useful to work in the corotating frame, defining a new azimuthal coordinate $\phi_{\rm rot}=\phi-\Omega_p t$. The conjugate momentum is then

$$p_{\phi_{\rm rot}}=\frac{mr^2}{2}(\dot\phi_{\rm rot}+\Omega_p)\sin^2\theta+p_\psi\cos\theta \tag{5}$$

and the conserved Hamiltonian is the Jacobi integral

$$J=\frac{p_\theta^2}{mr^2}+\frac{1}{mr^2}\frac{(p_{\phi_{\rm rot}}-p_\psi\cos\theta)^2}{\sin^2\theta}+\frac{p_\psi^2}{2mr^2}+V_g(r,\theta,\phi_{\rm rot}) - \Omega_p p_{\phi_{\rm rot}}. \tag{6}$$

We use these new variables and the corresponding equations of motion in our discussion of PRs in tumbling triaxial potentials, dropping the subscripts.

The gravitational potential energy $V(r,\theta,\phi)$ has two components: that due to the matter distribution in the galaxy, and that from the other wires making up the ring. We derive expressions for these below.

2.1 Torques due to the Galactic Potential

For triaxial systems, few explicit solutions of Poisson's equation are known: we choose a family of models where the density is stratified on similar concentric ellipsoids. Since galactic rotation curves in general, and those of PR systems in particular, are almost flat at large radii, the density ρ must fall off not faster than $1/r^2$. We consider models with

$$\rho(x,y,z)=\rho(\tilde{m}^2)=\frac{\rho_0}{1+\tilde{m}^2},$$
$$\tilde{m}^2=\frac{x^2}{a^2}+\frac{y^2}{b^2}+\frac{z^2}{c^2}, \quad (7)$$

where (a,b,c) specify the axis ratios and the size of the core within which the density is close to its central value ρ_0; $a\geqslant b\geqslant c$. The total mass inside the ellipsoidal radius $\tilde{m}$ is

$$M(\tilde{m})=4\pi abc\rho_0(\tilde{m}-\arctan\tilde{m}), \quad (8)$$

so the total mass of the spheroid diverges at large $\tilde{m}$. However, the classical theory of Chandrasekhar (1969) shows that shells of matter beyond ellipsoidal radius $\tilde{m}$ exert no force within that radius. Thus the forces we compute are the same as they would be if the density decreased more rapidly than prescribed by Eq. (7) beyond the outer limits of the PR, provided that the isodensity surfaces retain the same shape. We quote from de Zeeuw & Pfenniger (1988) the very simple form of the potential $\Phi_g(x,y,z)$ as expressed in confocal ellipsoidal coordinates

$$\Phi_g=F(\lambda)+F(\mu)+F(\nu), \quad (9)$$

where (λ,μ,ν) are the confocal ellipsoidal coordinates (de Zeeuw 1985) defined as the three roots of the cubic equation

$$\tilde{m}^2(\tau)=\frac{x^2}{a^2-\tau}+\frac{y^2}{b^2-\tau}+\frac{z^2}{c^2-\tau}=-1 \quad (10)$$

with $c^2\leqslant\nu\leqslant b^2\leqslant\mu\leqslant a^2\leqslant\lambda$. The integral for $F(\tau)$ given by de Zeeuw and Pfenniger's Eq. (2.13) has no closed form, but its derivatives can be expressed in terms of Carlson's (1979) incomplete elliptic integral of the third kind, available in standard numerical algorithm packages such as Numerical Recipes (Press *et al.* 1992)

$$\frac{\partial\Phi_g}{\partial\tau}=F'(\tau)=\frac{2}{3}\pi G\rho_0 abc R_J(a^2,b^2,c^2,\tau), \quad (11)$$

where

$$R_J(a^2,b^2,c^2,\tau)\equiv\frac{3}{2}\int_0^\infty\frac{dt}{(t+\tau)\sqrt{(t+a^2)(t+b^2)(t+c^2)}}. \quad (12)$$

The force components are elementary functions of the ellipsoidal coordinates when the matter distribution is oblate ($a=b$) or prolate ($c=b$): see Appendix B.

The energy of a wire of radius r and mass m with orientation given by (θ,ϕ) in this potential is given by integrating

$$V_g(r,\theta,\phi)=\int_{\text{wire}}\Phi_g dM=\frac{m}{2\pi}\int_0^{2\pi}\Phi_g(\lambda,\mu,\nu)d\eta, \quad (13)$$

where η measures the angle around the wire. The torque exerted by the potential on the precessing wire is found using the derivatives with respect to the orientation angles

$$\frac{\partial V_g(r,\theta,\phi)}{\partial(\theta,\phi)}=\frac{m}{2\pi}\int_0^{2\pi}\left(F'(\lambda)\frac{\partial\lambda}{\partial(\theta,\phi)}+F'(\mu)\frac{\partial\mu}{\partial(\theta,\phi)}+F'(\nu)\frac{\partial\nu}{\partial(\theta,\phi)}\right)d\eta; \quad (14)$$

we give formulas for the derivatives of the ellipsoidal coordinates with respect to the Euler angles (θ,ϕ) in Appendix A.

To reduce our computing time, we evaluated the torques by tabulating the function $F'(\tau)$ for values of $\tau\in[0,\lambda_{\max}]$, and using a spline function to interpolate. The number of points was such that the relative error is less than 10^{-6} throughout the range. We also used a spherical harmonic decomposition for the torque terms. When the potential is axisymmetric, the torque is clearly zero in the azimuthal ϕ direction; the θ torque was approximated as

$$\frac{\partial V_g}{\partial\theta}=m\sin\theta\sum_{i=0}^{n}A_i P_i(\cos\theta), \quad (15)$$

where the P_i are Legendre polynomials, and the A_i are constant coefficients. Since the potential is symmetric with respect to the equatorial plane, the torque is given purely by odd Legendre polynomials. Computing the terms of the series up to $i=9$ gives a fractional error of less than 10^{-5} for all inclinations θ in the most flattened halo we investigate ($c/a=0.5$).

In the case of a massive triaxial spheroid, the potential depends on the azimuthal angle ϕ; we may make a similar decomposition of the torque terms, but the coefficients are now functions of ϕ:

$$\frac{\partial V_g}{\partial\theta}=m\sin\theta[A_1(\phi)P_1(\cos\theta)+A_3(\phi)P_3(\cos\theta)+\cdots+A_9(\phi)P_9(\cos\theta)+\cdots], \quad (16)$$

$$\frac{\partial V_g}{\partial\phi}=m[A_0'(\phi)+A_2'(\phi)P_2(\cos\theta)+\cdots+A_8'(\phi)P_8(\cos\theta)+\cdots]. \quad (17)$$

The $A_i(\phi)$, up to $i=9$, were then approximated by a truncated series of the orthogonal set of functions $\cos 2j\phi$, $\sin 2j\phi$ as

$$A_i(\phi)=C_{i0}+C_{i1}\cos(2\phi)+\cdots+C_{ij}\cos(2j\phi)+\cdots+D_{i1}\sin(2\phi)+\cdots+D_{ij}\sin(2j\phi)+\cdots, \quad (18)$$

where C_{ij}, D_{ij} are defined as

$$C_{i0}=\frac{1}{2\pi}\int_0^{2\pi}A_i(\phi)d\phi, \quad (19)$$

$$C_{ij}=\frac{1}{\pi}\int_0^{2\pi}A_i(\phi)\cos(2j\phi)d\phi, \quad (20)$$

$$D_{ij}=\frac{1}{\pi}\int_0^{2\pi}A_i(\phi)\sin(2j\phi)d\phi; \quad (21)$$

a similar decomposition with coefficients C'_{ij}, D'_{ij} is defined for the $A'_i(\phi)$.

Evaluating the C, D coefficients up to $j=4$ gives a fractional error less than 10^{-5} for a moderately triaxial potential: $b/a=0.8$, $c/a=0.6$. These coefficients are found at the beginning of the calculation for the radius r corresponding to each wire, and stored for use in evaluating the torques at any tilt (θ,ϕ). We found that the above method gave better results than the reverse sequence of projection, taking the ϕ dependence first and the θ dependence second.

2.2 Mutual Interaction Between Massive Wires

The PR is divided into N concentric circular wires with radii r_i, masses m_i, and other quantities similarly labeled. The mutual potential energy of each pair of wires depends only on the angle α_{ij} between their planes, given by

$$\cos\alpha_{ij}=\cos\theta_i\cos\theta_j+\sin\theta_i\sin\theta_j\cos(\phi_i-\phi_j) \quad (22)$$

and can be found as follows. The gravitational potential due to a circular wire of mass m', radius r' lying in the $(\tilde{x},\tilde{y})$ plane is (e.g., Binney & Tremaine 1987, Sec. *2.6.2*)

$$\Phi(\tilde{x},\tilde{y},\tilde{z})=-\frac{2Gm'}{\pi}\frac{K(k)\sqrt{(1-k^2/2)}}{(r^2+r'^2)^{1/2}}, \quad (23)$$

where

$$k^2=\frac{4Rr'}{(r^2+r'^2+2Rr')}. \quad (24)$$

Here $K(k)$ is the first complete elliptic integral, and R is the cylindrical radius $R^2=\tilde{x}^2+\tilde{y}^2$, so that $r^2=R^2+\tilde{z}^2$. A second wire of radius r lying at an angle α to the first follows a curve $\tilde{z}=r\sin\eta\sin\alpha$, where η runs between 0 and 2π. The mutual potential energy is then

$$V_m(\alpha)=-\frac{Gmm'}{\pi^2(r^2+r'^2)^{1/2}}\int_0^{2\pi}K(k)\sqrt{1-k^2/2}\,d\eta, \quad (25)$$

where m is the mass of the second wire, and k is given as a function of η via expression (24) above. The torque between any two wires (i,j) follows by differentiating, and making use of the relation $E(k)=(1-k^2)d[kK(k)]/dk$:

$$\partial V_m(\alpha_{ij})/\partial\alpha_{ij}=\frac{Gm_im_jr_ir_j\sin 2\alpha_{ij}}{\pi^2(r_i^2+r_j^2)^{3/2}}\times 4\int_0^{\pi/2}\left(\frac{E(k)\sqrt{(1-k^2/2)}}{(1-k^2)}-K(k)\right)\times\frac{(1-k^2/2)^{3/2}}{k^2}\frac{\sin^2\eta\,d\eta}{\sqrt{1-\sin^2\alpha_{ij}\sin^2\eta}}. \quad (26)$$

The torques with respect to the angles $\{\phi_i,\theta_i\}$ are found from this equation, multiplying by $\partial\alpha_{ij}/\partial\theta_i$ or $\partial\alpha_{ij}/\partial\phi_i$.

In practice the integral of Eq. (26) is evaluated on a grid of points between $0>\eta>\pi/2$, for each pair of wires making up the ring. Since the integrand takes its largest value at $\eta=0$, becoming singular if k approaches unity, it makes sense to space the evaluation points more closely in that region when the wires have very similar radii. When $r_i-r_j=\Delta r$ and the tilt angle $\alpha_{ij}=\alpha$ are small, the integrand behaves as

$$h(\eta)\approx\frac{1}{\sqrt{2}}\left(\frac{\eta^2r^2\alpha}{\eta^2r^2\alpha^2+\Delta r^2}\right). \quad (27)$$

We space half our integration points between $\eta=0$ and $\eta=0.5\sqrt{\pi\Delta r/r\alpha}$, evenly in the variable

$$s=\frac{\arctan\eta r\alpha/\Delta r}{\arctan\pi r\alpha/2\Delta r}; \quad (28)$$

the other half of the integration points are spaced evenly in η over the remainder of the range.

The equations of motion (3) and (4) for each wire include such a contribution to the torque from each of the other wires; these $4N$ coupled differential equations specify the time development of the ring. In our numerical computation, we use units such that the gravitational constant $G=1=\rho_0$, the central density of the galaxy; lengths are measured in units such that the core radius a is close to unity.

3. SELF-GRAVITATING EQUILIBRIA

We search for equilibria in which the PR precesses steadily as a unit. In an axisymmetric galaxy, this means that all the wires must precess at the same rate $\dot{\phi}$, which can take a continuous range of values. In a triaxial potential, the precession speed of the ring *must match* the tumble rate Ω_p of the potential so that the two remain in phase. Thus in contrast to the oblate case, in a triaxial potential with a given Ω_p there are only a few possible equilibria for each set of rings specified by $\{m_i,r_i\}$.

The requirement that all wires maintain a constant inclination is that $p_\theta=\dot{p}_\theta=0$ for each of them; the second of these implies that the precession speed in the inertial frame is given, from Eq. (3), by

$$(mr^2/2)\dot{\phi}^2\cos\theta\sin\theta-\dot{\phi}\sin\theta p_\psi-\frac{\partial V(r,\theta,\phi)}{\partial\theta}=0. \quad (29)$$

For steady precession, $\ddot{\phi}=0$ which, since the inclination is constant, implies $\dot{p}_\phi=0$; there must be no torque about the axis z on any of the wires. In an oblate potential this last condition is always satisfied when the wires all have the same azimuthal $\phi_i=\phi$, since the inter-ring torque then lies purely in the (x,y) plane, and the galaxy exerts no azimuthal torque. When the potential has triaxial symmetry, an equilibrium with all the wires at constant azimuth is possible only when the lines of nodes lies along one of the principal axes: we require $\phi=0$ or $\phi=\pi/2$. Equation (29) then yields N coupled equations for the angles θ_i in terms of the ring precession rate $\dot{\phi}$ or the tumbling speed Ω_p of the galaxy.

Following Sparke (1986), we first investigate these equilibria and their stability using the very simplest model of a PR, consisting of only two wires; we label these by "primed" and "unprimed" quantities. When the galaxy potential is triaxial the coordinate $\phi+\phi'$ is no longer cyclic, so we cannot use the same method, of searching for min-

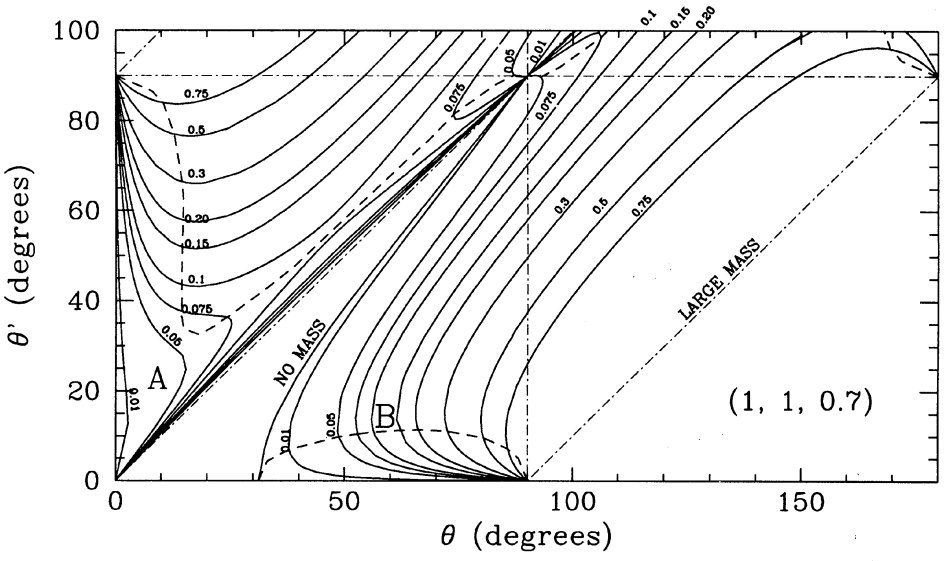

FIG. 1. The inclination θ, θ' for a pair of steadily precessing concentric massive wires in an oblate model with axis ratios 1:1:0.7. Along each solid curve the mass of the wires is kept constant, while the ring precession rate varies. Regions of secular stability are bounded by dashed lines; the two families A and B are discussed in the text. No solutions exist between the line $\theta=\theta'$ (wires coplanar but tilted) and the "no mass" line, or in the triangle at the lower right. The wires have radii of 5.75 and 7.25 units with equal mass (i.e., with linear density decreasing as $1/r$). Curves are labeled by the combined mass m_r of the wires, in units of the galactic m_g within the elliptic radius at the outer wire.

ima in the Hamiltonian, to check the stability of an equilibrium state. Instead, we linearize the equations of motion about the equilibrium configuration and then look for solutions with an exponential dependence on time: $\theta(t)=\theta_0+\Delta\theta\exp(\lambda t)$,..., etc.

Close to an equilibrium, the perturbed equations of motion for $(\theta,\phi,p_\phi,p_\theta)$ take the form

$$\begin{aligned}
\dot\theta &= \frac{\partial^2 T}{\partial p_\theta^2}\Delta p_\theta,\\
\dot\phi &= \frac{\partial^2 T}{\partial p_\phi \partial\theta}\Delta\theta+\frac{\partial^2 T}{\partial p_\phi^2}\Delta p_\phi,\\
\dot p_\theta &= -\frac{\partial^2 V}{\partial\theta^2}\Delta\theta-\frac{\partial^2 V}{\partial\theta\partial\phi}\Delta\phi-\frac{\partial^2 T}{\partial\theta\partial p_\phi}\Delta p_\phi-\frac{\partial^2 V}{\partial\theta\partial\theta'}\Delta\theta'\\
&\quad -\frac{\partial^2 V}{\partial\theta\partial\phi'}\Delta\phi',\\
\dot p_\phi &= -\frac{\partial^2 V}{\partial\phi\partial\theta}\Delta\theta-\frac{\partial^2 V}{\partial\phi^2}\Delta\phi-\frac{\partial^2 V}{\partial\phi\partial\theta'}\Delta\theta'-\frac{\partial^2 V}{\partial\phi\partial\phi'}\Delta\phi',
\end{aligned} \tag{30}$$

where T, V indicate the contribution to the Hamiltonian from kinetic and potential energy terms, respectively. There are four similar equations for the primed quantities. The derivatives, taken at the unperturbed equilibrium point, are the entries in the matrix M specifying the time derivatives of the perturbation quantities as a linear function of those quantities; we evaluated most of these derivatives, and found the eigenvalues of M, numerically. Because the system is time reversible, the characteristic equation for λ involves only λ^2; if λ is a root, so is $-\lambda$. The equilibrium configuration for the two wires is stable if λ^2 is real and negative; the perturbed system will oscillate about the equilibrium. If any root has a nonzero real part, the solution will contain a term growing exponentially in time; the wires rapidly move away from the equilibrium configuration.

3.1 *Equilibria in an Oblate Galaxy*

The results for a two-wire model in the pseudoisothermal potential with axes $(a,b,c)=(1,1,0.7)$ are illustrated in Fig. 1. Here the wires have radii $r=5.75$ and $r'=7.25$ units, with equal masses. The curves in the diagram are labeled by the ratio of the combined mass $m+m'=m_r$ of the wires to the galactic mass m_g within the elliptic radius 7.25 at the outer edge of the ring; $m_g=51.16$ in our units. Along these curves the precession rate $\dot\phi$ varies continuously, but not monotonically. Regions of stable equilibria are bounded by the dashed curves. This diagram is symmetric under reflection through the point (90°,90°), since this amounts to reversing the spin of both wires. It is to be compared with Fig. 2 of Sparke (1986); we describe the solution families for comparison with the triaxial case.

For each value of the ring mass m_r there are two solution curves. The first family of curves (A: "warp-up" solutions) includes the point (0°,0°); the unprimed inner wire lies closer to the equatorial plane while the outer is tipped toward the pole. The second (B: "warp-down") starts from (90°,0°): here the inner wire is found nearer to the pole. Along the solution curves through (0°,0°) belonging to the warp-up family A, if the mass m_r falls below a certain value—here about $0.075m_g$—then the inner wire has a maximum tilt: as the outer wire becomes more inclined, the inner one falls back to the equatorial plane. For

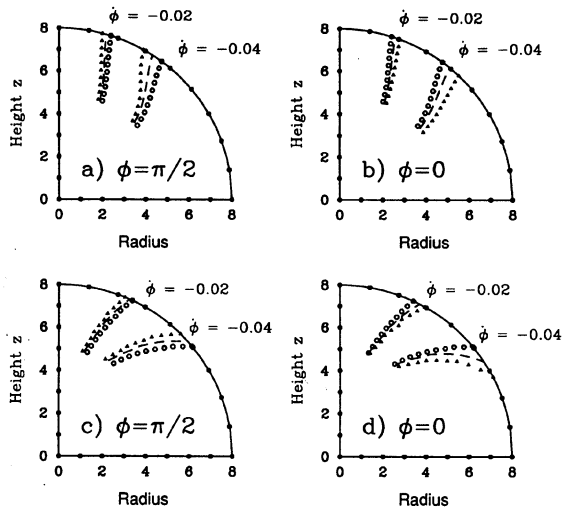

FIG. 2. The equilibrium states of a model consisting of 10 wires distributed evenly between radii of 5 and 8 units, for two values of the ring precession rate $\dot{\phi}$ relative to inertial space. Open circles indicate the equilibria evaluated in the oblate pseudoisothermal potential with axis ratios 1:1:0.7, dashes indicate those in the triaxial case 1.0253 : 0.9740 : 0.7, and filled triangles indicate those for the most triaxial case 1.0512 : 0.9460 : 0.7. (a) shows the stable upward-warping equilibria with $m_r=0.1m_g$, and $\phi=\pi/2$; (b) shows the corresponding unstable equilibria with $\phi=0$. (c) shows down-warping equilibria with $m_r=0.005m_g$ and $\phi=\pi/2$, and (d) shows the corresponding unstable solutions for $\phi=0$.

larger masses, the angle between the wires reaches a maximum at some intermediate tilt, and then declines as both wires become nearly polar. Mutual torques equalize the precession rates of the two wires; the outer wire at higher inclination tends to slow the regression of the inner one, while itself regressing more rapidly than it would in the galactic field alone, so that the two wires precess together as a unit. The equilibria approach the curve $\theta=\theta'$ as the ring mass grows: self-gravity becomes so strong that the galactic potential is irrelevant.

When the ring has very little mass, the two wires move nearly independently in the galactic potential; in solutions of family B, the inner wire must be more nearly polar to equalize the precession rates. The two wires are close to coplanar at the pole, but the angle between them increases near the equator: when the outer wire is almost equatorial, the inner wire is tilted by about 30°. As the ring mass grows, the difference in tilts grows larger, since the inner wire tugs on the outer, slowing its regression. Thus the outer wire must become more nearly equatorial so as to increase the regression caused by the galactic field, and at the same time the inner wire must become more polar; at a given precession rate, the wires diverge as the ring mass grows. When the ring is heavy enough, the angle θ may exceed 90°; the inner wire has the z component of its spin reversed. If the combined mass $m_r \geqslant 0.05m_g$, then there are equilibria with the two wires lying on opposite sides of the pole. At large ring mass these curves approach the limit $\theta=\theta'+90°$, with the two wires perpendicular.

When the ring has zero mass, the solutions of both these families are neutrally stable. When self-gravity is strong enough, equilibria of family A with the two wires almost coplanar become stable: the mutual potential energy is near a minimum there. Some states in which the inner ring lies near the equatorial plane are also stable: these are related to the type I warping modes of galaxy disks discussed by Sparke & Casertano (1988). The warp-down equilibria of sequence B are stable only if the outer ring is very close to the equatorial plane: these are related to the type II warps of Sparke & Casertano (1988).

Stable solutions with both wires near the pole are of the greatest relevance for the observed polar ring systems. These have $\theta' > \theta$, so that the outer wire is more steeply inclined, and $\theta \simeq \theta'$; the ring is not greatly warped. Such stable equilibria exist only when the total ring mass is larger than the critical value $m^*=0.05m_g$. For masses just above m^*, there are stable equilibria near the pole and near the equatorial plane, but not at intermediate angles: if the mass is larger (here $m^* > 0.075m_g$), there are stable solutions at any angle to the pole. Since the potential is oblate, all equilibria correspond to precession which is retrograde relative to the total z-angular momentum of the ring. Equation (29) can be used to compute equilibria for models consisting of many wires. Figure 2 shows cross sections through equilibria computed using a 10 wire model, in the same potential as for Fig. 1 and for two values of the precession rate; these curve gently up to the pole. Direct numerical integration shows them to be stable.

3.2 Equilibria in a Tumbling Triaxial Galaxy

In a triaxial potential, we require that the precession speed of the ring must match the tumble rate Ω_p of the potential about its short axis z, and that the line of nodes should lie along one of the principal axes. We first consider equilibria with $\phi=\pi/2$, such that the ring cuts the (x,y) plane of the galaxy on the intermediate, y axis. This is the same line along which the stable anomalous retrograde orbits (Schwarzschild 1982; Heisler *et al.* 1982, Tohline & Durisen 1982, Magnenat 1982, Mulder & Hooimeyer 1984) intersect the (x,y) plane, and where the potential energy of each wire is a minimum in the galactic potential for fixed inclination θ.

We consider a series of triaxial models with constant oblateness, in the sense that $c^2/(a^2+b^2)$ is held equal to its value in the axisymmetric potential of Fig. 1. Figure 3 shows the stability diagram for the two-wire model in a triaxial potential with $(a,b,c)=(1.0253,0.9740,0.7)$; the triaxially parameter $T\equiv(a^2-b^2)/(a^2-c^2)=0.18$. The solid lines again show equilibria for a fixed value of the ring mass, while the tumble speed Ω_p of the potential varies along each curve; their appearance is not very different from that of Fig. 1. The solid curves are symmetric under reflection through the point (90°,90°), while Ω_p reverses its sign. The dotted lines represent sequences of equilibria where Ω_p is kept constant while the ring mass varies, and regions of stability are bounded by dashed lines.

The solution curves are much the same as those found in the oblate case. The stability properties of the A warp-up

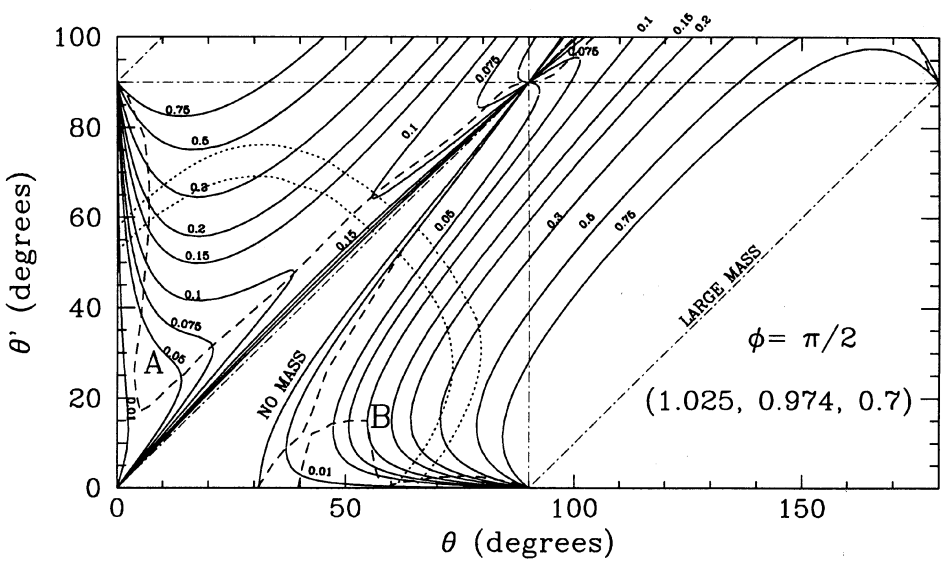

FIG. 3. As in Fig. 1, but for equilibrium states in a tumbling triaxial model with axis ratios 1.0253 : 0.9740 : 0.7. The ring mass is constant along the solid lines, while the tumble speed of the potential varies; regions of secular stability are bounded by dashed lines. The dotted lines show loci of constant precession speed: $\Omega_p = -0.03$ on the outer curve, while $\Omega_p = -0.035$ on the inner.

family of solutions are also similar; solutions close to the $\theta' = \theta$ curve are stable, as are the "equatorial warp" solutions, in which the inner ring is almost on the equator and the outer one is tipped toward the pole, with a large angle between the two rings. Stable solutions appear when the ring mass exceeds $m^* \simeq 0.06 m_g$; slightly more mass is needed to stabilize this configuration than in the oblate case. The stable equilibria of the B family now include those for zero mass; these have exactly the orientations of the anomalous retrograde orbits (Steiman-Cameron & Durisen 1984). Stable equilibria now exist in a narrow strip along the "no mass" curve when $m_r < 0.02 m_g$. Two further areas of stability are centered around (48°,7°), and in a narrow strip around (0°,75°) where the outer ring is almost in the equatorial plane, and the inner ring close to polar.

Figure 4 presents a similar diagram for a more triaxial model with axes (1.0512,0.9460,0.7); $T = 0.34$. Here the stable equilibria of the A family have split into two regions: a strip near $\theta = \theta'$, where stable solutions appear when the ring mass exceeds $m^* \simeq 0.1 m_g$, and another region where the inner wire tilts by at most $\sim 7°$ from the equatorial plane. In the B family, the stability band along the "no mass" line has widened by comparison with that in the

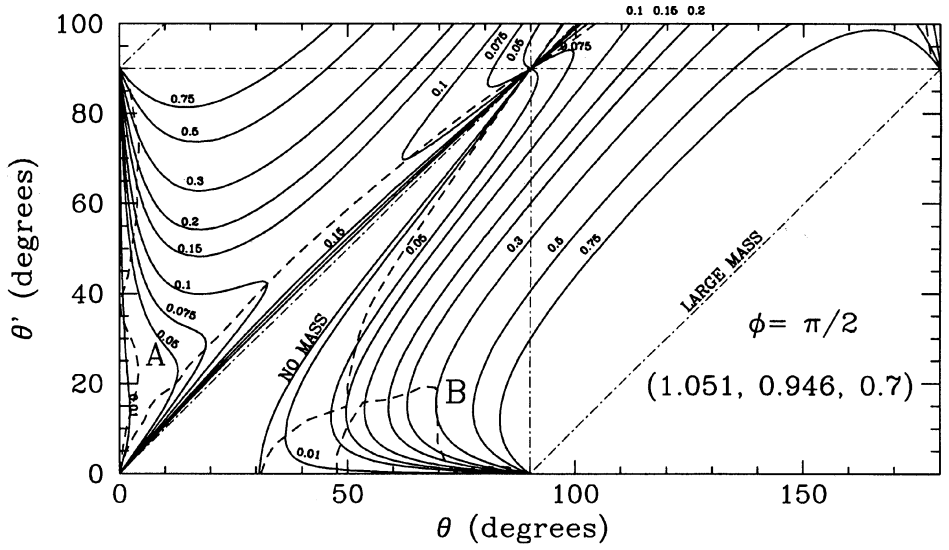

FIG. 4. As in Fig. 3, but for a tumbling triaxial model with axis ratios 1.0512 : 0.9460 : 0.7.

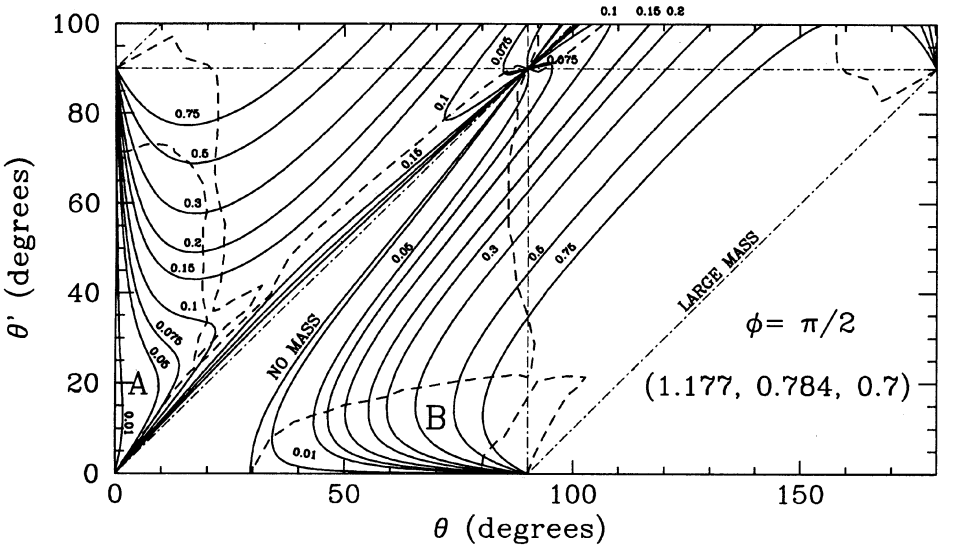

FIG. 5. As in Fig. 3, but for a tumbling triaxial model with axis ratios 1.177 : 0.784 : 0.7.

previous, less triaxial, case: stable solutions now exist for $m_r < 0.07 m_g$. The stable region with the outer ring close to the equatorial plane is wider than in Fig. 3; the tiny strip of stability with nearly orthogonal wires is present as well.

Figure 5 shows the equilibria for a near-prolate model, with axes (1.177,0.784,0.7) and $T=0.88$. The near-coplanar equilibria of family A remain stable, but solutions with the inner ring close to the equator are now unstable unless the outer ring is very nearly polar. A "tongue" of stable equilibria with $\theta \approx 20°$ extends downward from (0°,90°). In the B family, the region of stable solutions adjoining the no mass line is enlarged, particularly at intermediate inclinations, while stable equilibria with $\theta' \approx 0$ are now restricted to very high ring masses.

The equilibria most relevant to polar ring dynamics are those with the two wires nearly coplanar. In an oblate potential, only upward-curving solutions of this type can be stable; the outer ring must be closer to the pole. In the triaxial potential, downward-curving equilibria are stabilized. As the ring becomes more massive, a smaller set of the downward-curving equilibria is stable, while a larger fraction of the upward-bending solutions become so. The precession of all the equilibria, and hence the tumbling of the triaxial figure, is retrograde with respect to the total z-angular momentum of the ring.

We can proceed similarly to find equilibria with $\phi=0$; the ring now circles the short and the intermediate axes of the galaxy, such that each wire has its maximum potential energy at a given inclination. The solution curves are again not very different from those in the oblate potential. However, there are no stable orbits about the intermediate axis of a triaxial potential which tumbles about its short axis (Heisler *et al.* 1982), and we are not surprised to find that all the equilibria of our two-wire model are unstable.

Figure 2a compares the shapes of the upward-curving solutions in our near-oblate potentials for a ten-wire model with $\phi=\pi/2$; these equilibria have very similar shapes to the corresponding solutions in the oblate potential, but are somewhat closer to polar at a given precession speed. Numerical integration of the equation of motion shows them to be stable. The similar but unstable solutions with $\phi=0$ [Fig. 2(b)] lie closer to the equatorial plane than those with $\phi=\pi/2$. Figures 2(c) and 2(d) show downward-warping equilibria with the same precession rates but for mass $m_r=0.005 m_g$. The solutions of Fig. 2(c) with $\phi=\pi/2$ are unstable in the oblate potential; in the triaxial potential with axes (1.0253,0.9740,0.7), the equilibrium with $\dot{\phi}=-0.02$ is unstable while that with $\dot{\phi}=-0.04$ is stable; equilibria with both values of the precession speed are stable in the more triaxial potential with axes (1.0512,0.9460,0.7). All the solutions of Fig. 2(d) are unstable.

We have not considered many dissipative effects in these calculations. However, previous gas-dynamical simulations (reviewed by Christodoulou *et al.* 1992) show that dissipation does not cause a polar ring around an oblate galaxy to collapse into the center or to settle significantly toward the equator within a Hubble time, unless the galaxy potential is so flattened that the mass distribution must be almost disklike. Otherwise, the ring can maintain a coherently precessing structure, in which the influence of gas–gas collisions is small. This suggests that the stable rigidly precessing configurations which we discuss here should not be rapidly disrupted by gas processes. Some of the equilibria which are unstable in a purely gravitating system may be stabilized in a gaseous ring: this process appears to occur for downward-warping states in the oblate-galaxy simulations of Katz & Rix (1992).

4. TIME-EVOLVING POLAR RINGS

In an oblate galaxy potential, even if self-gravity does not lock a polar ring into a steady state, it can still cause the characteristic warp up toward the pole. This is because both the energy and the total z-angular momentum of the ring must be conserved; if it is energetically favorable for the inner part of the ring to sink toward the equator, increasing its z-angular momentum at the expense of the outer portion, then a warp toward the pole will develop.

A simple calculation shows that this is the case for a low-mass ring consisting of two wires, far outside the core of a slightly oblate galaxy. Let the inner wire have radius r, mass m, and be tilted by an angle θ away from the equatorial plane, with the azimuth of the line of nodes at angle ϕ, while the outer wire has radius r', mass m', and tilt angles θ',ϕ'. We show in Appendix B that far from the core, the torque from the galaxy loses its radial dependence and becomes a function only of the inclination θ. When the galaxy is not too strongly flattened, the leading term $A_1 \sin\theta\cos\theta$ of the expansion (15) is a good approximation to the torque term; $A_1>0$ for an oblate galaxy. Then the energy is given, to within a constant term, by

$$E=T-(A_1/2)(m\cos^2\theta+m'\cos^2\theta') + V_m(\theta,\theta',\phi-\phi'), \quad (31)$$

where the first term is the kinetic energy of the two wires, the middle term represents the potential energy of the wires in the galaxy potential, and V_m is the mutual potential energy. If the ring is light, then the term in V_m is small compared to the others, since it is quadratic rather than linear in the ring mass. The wires precess slowly in the mildly aspherical galaxy potential, so the total z-angular momentum is

$$J_z \approx mr^2\Omega(r)\cos\theta+m'r'^2\Omega(r')\cos\theta'; \quad (32)$$

far outside the core, the rotation curve becomes flat and $r\Omega(r)$ is asymptotically constant. Then in any motion

$$\Delta E=0\approx\Delta(T)-A_1 m\Delta(\cos\theta)[\cos\theta-(r/r')\cos\theta']. \quad (33)$$

If the ring is initially static in its orientation, the kinetic energy can only increase; if it starts nearly coplanar ($\theta\approx\theta'$), then because $r'>r$, any motion requires $\Delta(\cos\theta)>0$, and the tilt of the inner wire must decrease. Thus the transfer of energy and angular momentum between the wires due to self-gravity—or indeed any weak coupling—causes the outer wire to be pushed up toward the pole, while the inner wire settles toward the equator. For a multiwire ring, extending inward to a few times the galaxy core radius, explicit computations are required: these show similar behavior. As an example, Fig. 6 shows the evolution of an initially coplanar ring in the oblate potential of Fig. 1; the ring splits into three parts, with the outermost wires thrown up toward the pole, while the inner wires sink to lower inclination.

This effect, of making the outer parts of the ring more nearly polar than the inner regions, appears similar to what

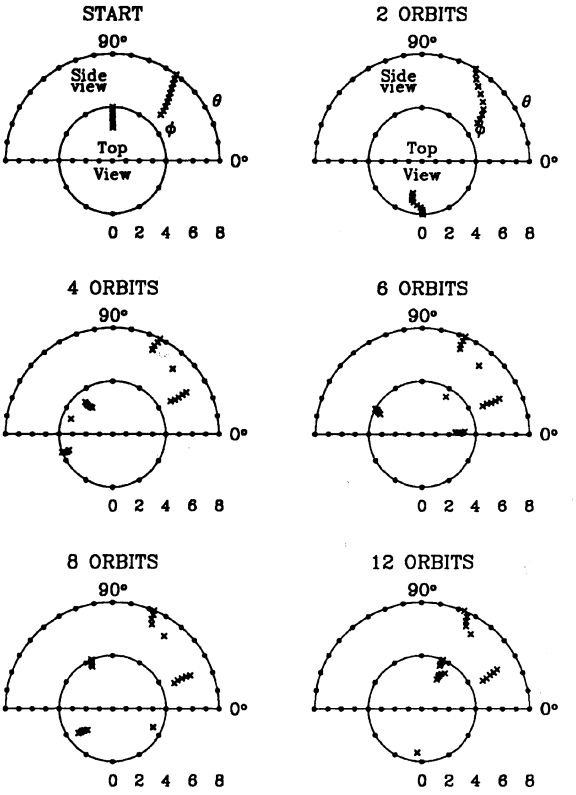

FIG. 6. Time evolution of an unstable polar ring in the oblate potential of Fig. 1, followed using the 10-wire model of Fig. 2. The initial tilt angles are given by the equilibrium state of Fig. 2(a) with $\dot{\phi}=-0.04$, but the ring mass is reduced to $m_r=0.08m_g$. At each stage, the outer semicircular frame shows the ring inclination θ as a function of radius (horizontal scale); the inner frame gives the azimuth ϕ, with the radial scale shrunk to half that of the outer frame. Time is given in units of the orbital period at $r=8$ (18.84 of our computational units). The ring is unstable and breaks up into subrings.

happens when dissipative processes cause an initially inclined ring to settle toward the equatorial plane of an oblate galaxy potential. Dissipation is fastest at small radii, where the orbital periods are short, so the inner part of the ring will be the first to reach the equatorial plane, while the outer disk is still highly inclined (e.g., Steiman-Cameron & Durisen 1988). Since dissipative settling depends on differential precession, the ring is expected to be twisted; a self-gravitating ring may or may not develop a twist, depending on the strength of the self-coupling. However, the two mechanisms are physically quite different—self-gravity causes energy and angular momentum to be transported within the ring structure, while dissipative settling is essentially a local process which reduces the total energy of the system.

Eventually, an unstable ring will break up into a number of subrings which precess independently; the outer ring material is pushed into an orbit closer to the pole than the original ring plane, while inner gas sinks toward the equator of the S0 or elliptical galaxy. Thus a single accreted gas cloud might give rise to a multiple ring system, such as that seen in ESO 474−G26 (SWR). However, dissipative pro-

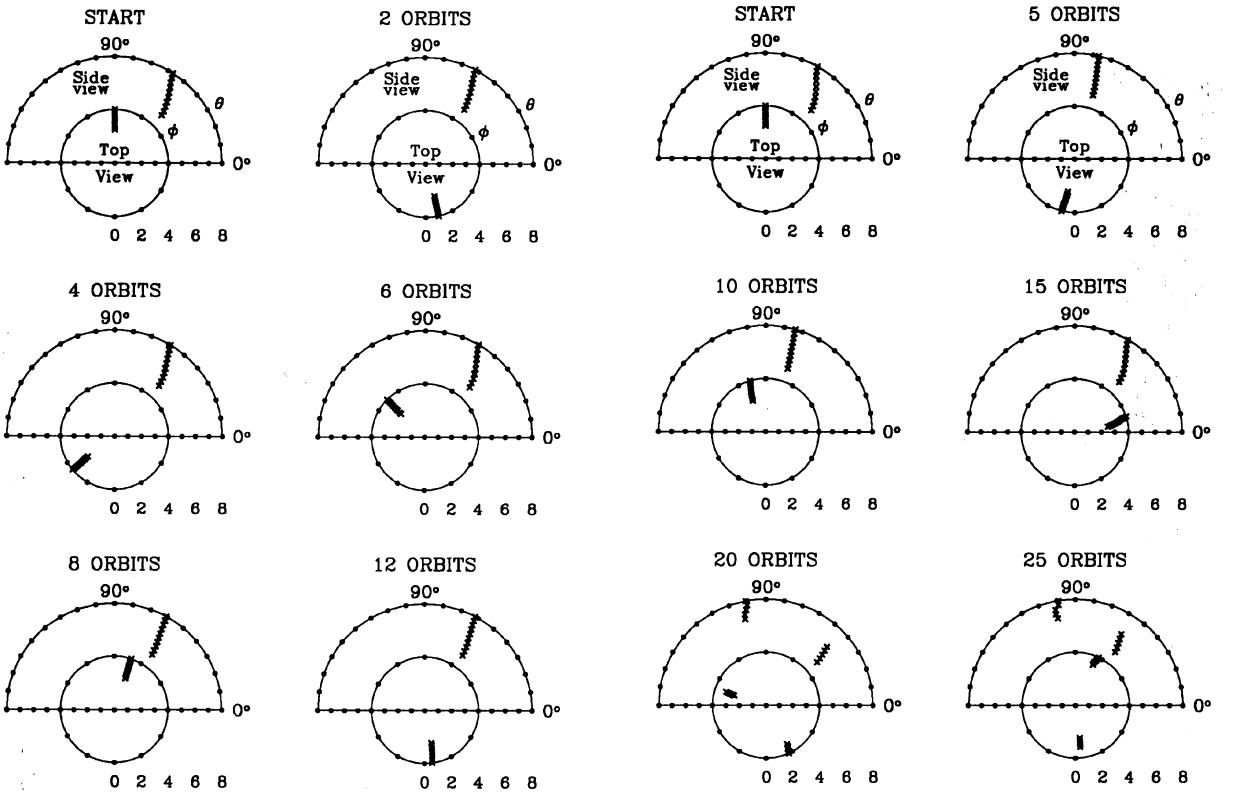

FIG. 7. The upward-warping equilibrium ring of Fig. 2(a) (with $\phi=\pi/2$) in the triaxial potential with axis ratio 1.0253 : 0.9740 : 0.7, tumbling at the rate $\Omega_p=-0.04$, when placed in the corresponding stationary potential. The structure wobbles gently due to the azimuthal torque of the galactic potential.

FIG. 8. As in Fig. 7, but for the more triaxial model with axis ratio 1.0512 : 0.9460 : 0.7. The structure is unstable and breaks up.

cesses act more rapidly at smaller radii and lower inclinations to remove ring gas; if the inner material disappears completely, the remaining ring will be thinner and in a more nearly polar orbit than that on which the gas was originally accreted. This might resolve a puzzle pointed out by SWR: why so many polar rings are so nearly polar, when the initial orbits of the captured material must have been much more uniform in angle.

In a triaxial potential, the ring will only be in equilibrium if it precesses at the same speed with which the galaxy potential is tumbling. The precession rate depends on the oblateness of the potential, and on an average over the ring inclination, which are quantities independent of the galaxy tumble rate; hence of all possible configurations for near-polar rings in triaxial potentials, most will be far from equilibrium. However, if its mass is large enough and the triaxality not too pronounced, the ring can effectively ignore the nonaxisymmetry of the galaxy; it precesses at an average rate appropriate to its inclination in the azimuthally averaged potential, while oscillating about a state close to where the stable upward-warping equilibrium would be in that oblate potential. Figure 7 shows that a ring of mass $0.1m_g$ with the initial tilt and velocity appropriate to a stable upward-warping equilibrium in the triaxial potential corresponding to Fig. 3 (axis ratio 1.0253 : 0.9740 : 0.7) tumbling with $\Omega_p=-0.04$ (as shown in Fig. 2), wobbles gently when placed in the stationary potential with the same parameters, while still precessing about the z axis at an average rate $\dot{\phi}\approx-0.04$. But when a ring of the same mass with the equilibrium parameters appropriate to the more triaxial mass distribution of Fig. 4, with again $\Omega_p=-0.04$, is placed in the stationary potential, it breaks apart: Fig. 8.

We find no corresponding downward-warping pseudoequilibria, with shapes close to those of the stable solutions; an initially downward-bending ring falls apart if the potential is not precessing at close to the appropriate rate. Figure 9 shows the time development of a ring with $m_r=0.005m_g$ which has initially the configuration of a stable downwarp equilibrium in the potential of Fig. 4 with $\dot{\phi}=-0.02$, when it is placed in the corresponding stationary potential; part of the ring is thrown up over the pole, and the structure disintegrates. This is not unexpected, since in the oblate potential, all the downward-warping near-coplanar ring equilibria are unstable.

5. SUMMARY

We have shown that PRs around a triaxial potential tumbling about its short axis can be stabilized by self-gravity, in much the same way as rings around an axisymmetric oblate galaxy. The precession rate of an equilibrium

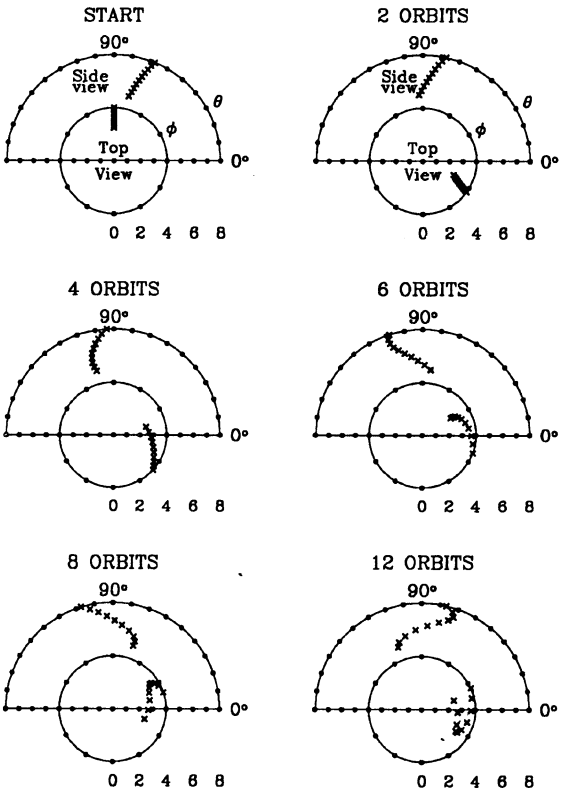

FIG. 9. As in Fig. 7, for the stable downward-warping ring of Fig. 2(c) with $m_r=0.005m_g$ and $\Omega_p=-0.02$, in the model with axis ratio 1.0512 : 0.9460 : 0.7. When placed in the stationary potential, the ring breaks up.

ring around an oblate galaxy depends on the off-axis angular momentum of the ring; so for each ring mass, there is a continuum of possible equilibria. In the triaxial case, we need to lock the precession of the ring, which is retrograde with respect to the z component of the ring angular momentum, into the tumbling of the figure. Thus in a given potential, for a given mass distribution in the ring, only a few discrete equilibrium solutions are possible.

We have investigated solutions in which the ring has no sense of twisting; then, the line of nodes, along which each orbit in the ring cuts the equatorial plane of the galaxy, must lie along one of the principal directions. All the equilibria in which the line of nodes coincides with the long axis are unstable; this is as expected, since in a triaxial potential tumbling about its short axis, there are no stable orbits about the intermediate axis. When the line of nodes lies along the intermediate axis, there are two types of stable solutions. Rings with a mass above some minimum value can be in stable equilibria similar to those in an oblate potential, with the ring warping up toward the pole. When the ring mass is less than some maximum value, there are stable solutions which warp down toward the equatorial plane; for zero mass, the warped ring plane coincides with that of the anomalous retrograde orbit family. The stable upward-warping solutions can be regarded as arising from the ring's self-gravity, while the stable downwarp solutions are due to the triaxiality of the potential; accordingly, the mass range occupied by the former shrinks, and that of the latter grows, as the galaxy shape deviates further from axisymmetry.

Although there is only a very restricted set of true equilibrium states, if the ring is sufficiently massive and the triaxiality not too strong, it can oscillate in a quasiperiodic motion, with an average precession rate set by the azimuthally averaged potential. Dynamical theory (e.g., Lichtenberg & Lieberman 1983) implies that this oscillation takes place about a true periodic orbit, in which the ring is as close as possible to a self-gravitating equilibrium state in the oblate component of the potential, but is slightly disturbed as its precession takes it around the triaxial potential. It would be hard to distinguish observationally between such an oscillating structure and a steadily precessing equilibrium ring.

Thus if the flattening of the potential could be constrained independently, the presence of an apparently stable polar ring would give a bound on the triaxiality of the underlying mass distribution. The limits obtained would depend on the assumed mass and surface density of the ring; neutral hydrogen observations provide a lower bound on the mass. Candidates for such an analysis include the narrow PRs, which lie within the optical body of the central galaxy where it is expected that luminous material dominates the gravitational potential, and systems where the flattening of the dark material can be estimated by methods such as those of Sackett & Sparke (1990).

Part of this work was done when one of us (M.A.) was visiting the Department of Astronomy of the University of Wisconsin-Madison and at Padova: the heads of the respective departments are thanked. M.A. would like to acknowledge the "Sandra and Enea Mattei" Foundation for partial financial support, and I.S.A.S. (Trieste), where she did part of this work as a component of her Ph.D. thesis. L.S.S. was partially supported by the National Science Foundation (AST-92-20650) and by the Graduate School of the UW-Madison. M.A. Acknowledges stimulating discussions with Professor M. Capaccioli, and Professor G. Galletta. Both authors would like to thank Professor D. W. Sciama for his hospitality at I.S.A.S., in the month of 1992 November, and to thank Professor P.T. de Zeeuw, our referee, for a helpful report and the suggestion that we include Fig. 5.

APPENDIX A: DERIVATIVES OF (λ,μ,ν) WITH RESPECT TO (θ,ϕ)

A point with angle coordinate η on a ring with orientation angles (θ,ϕ) has Cartesian coordinates

$$x=r(\cos\eta\cos\phi-\sin\phi\sin\eta\cos\theta), \quad \text{(A1)}$$

$$y=r(\cos\eta\sin\phi+\cos\phi\sin\eta\cos\theta), \quad \text{(A2)}$$

$$z=r\sin\eta\sin\theta. \quad \text{(A3)}$$

To find the derivatives of the corresponding ellipsoidal coordinates (λ,μ,ν) with respect to (θ,ϕ), we use the following relations from Eq. (10):

$$\lambda+\mu+\nu=a^2+b^2+c^2+r^2 \tag{A4}$$

which is constant since the radius r of the precessing ring is fixed, and

$$\begin{aligned}\lambda\mu+\mu\nu+\nu\lambda\equiv B&\\ =a^2b^2+c^2b^2+a^2c^2+a^2(r^2-x^2)&\\ +b^2(r^2-y^2)+c^2(r^2-z^2),&\end{aligned} \tag{A5}$$

$$\lambda\mu\nu\equiv -C=a^2b^2c^2+a^2b^2z^2+x^2b^2c^2+a^2c^2y^2. \tag{A6}$$

As (θ,ϕ) vary we can write the change in the ellipsoidal coordinates in terms of changes in B, C,

$$\Delta\lambda=\frac{(\nu-\mu)[\lambda\Delta B-\Delta(-C)]}{\nabla}, \tag{A7}$$

$$\Delta\mu=\frac{(\lambda-\nu)[\mu\Delta B-\Delta(-C)]}{\nabla}, \tag{A8}$$

$$\Delta\nu=\frac{(\mu-\lambda)[\nu\Delta B-\Delta(-C)]}{\nabla}, \tag{A9}$$

where

$$\nabla=\lambda^2(\mu-\nu)+\mu^2(\nu-\lambda)+\nu^2(\lambda-\mu). \tag{A10}$$

The increments in B,C can in turn be expressed in terms of $\Delta(x^2-y^2)$ and $\Delta(z^2)$:

$$\Delta B=\left(\frac{(a^2+b^2)}{2}-c^2\right)\Delta(z^2)-\frac{(a^2-b^2)}{2}\Delta(x^2-y^2), \tag{A11}$$

where the coefficient of $\Delta(z^2)$ is a measure of the oblateness, while that of $\Delta(x^2-y^2)$ is related to the nonaxisymmetry of the potential. Similarly

$$\begin{aligned}\Delta(-C)=&\left(a^2b^2-c^2\frac{(a^2+b^2)}{2}\right)\Delta(z^2)\\ &-c^2\frac{(a^2-b^2)}{2}\Delta(x^2-y^2).\end{aligned} \tag{A12}$$

The increment

$$\Delta(z^2)=-2r^2\sin^2\eta\cos\theta\Delta(\cos\theta) \tag{A13}$$

depends only on the θ angle, while $\Delta(x^2-y^2)$ is a function of both (θ,ϕ):

$$\begin{aligned}\frac{\partial(x^2-y^2)}{\partial(\cos\theta)}=&-2r^2\sin\eta(\cos\theta\cos 2\phi\sin\eta\\ &+\sin 2\phi\cos\eta),\end{aligned} \tag{A14}$$

$$\begin{aligned}\frac{\partial(x^2-y^2)}{\partial\phi}=&-2r^2[\sin 2\phi(\cos^2\eta-\cos^2\theta\sin^2\eta)\\ &+\cos 2\phi\cos\theta\sin 2\eta].\end{aligned} \tag{A15}$$

When the potential is oblate $(a=b)$, the potential depends only on (λ,ν) which are independent of ϕ. The equations analogous to Eqs. (A4) and (A5) give

$$\frac{\partial\lambda}{\partial\theta}=\frac{r^2(a^2-c^2)\sin^2\eta\sin 2\theta}{\nu-\lambda}=-\frac{\partial\nu}{\partial\theta}. \tag{A16}$$

In the prolate case, we have $b=c$, and $\Delta\lambda=-\Delta\mu$:

$$(\mu-\lambda)\Delta\lambda=(\lambda-\mu)\Delta\mu=(c^2-a^2)\Delta x^2, \tag{A17}$$

so that derivatives of (λ,μ) depend only on

$$\begin{aligned}\frac{\partial x^2}{\partial\theta}=&-r^2\sin\theta[\cos\theta\sin^2\eta(1-\cos 2\phi)\\ &-\sin 2\phi\cos\eta\sin\eta],\end{aligned} \tag{A18}$$

$$\begin{aligned}\frac{\partial x^2}{\partial\phi}=&r^2[\sin 2\phi(\cos^2\theta\sin^2\eta-\cos^2\eta)\\ &-\cos\theta\sin 2\eta\cos 2\phi].\end{aligned} \tag{A19}$$

APPENDIX B: TORQUE FAR OUTSIDE THE CORE OF A SLIGHTLY OBLATE HALO

The potential of the oblate distribution $(a=b)$ is given by Eqs. (2.29) and (2.30) of de Zeeuw & Pfenniger (1988):

$$\Phi_g=F_1(\lambda)+F_1(\nu), \tag{B1}$$

$$\begin{aligned}F_1'(\tau)=&\frac{f(\tau)-f(a^2)}{\tau-a^2},\\ f(\tau)=&-\frac{2\pi G\rho_0a^2c}{\sqrt{\tau-c^2}}\arctan\sqrt{\frac{\tau-c^2}{c^2}}.\end{aligned} \tag{B2}$$

The torque on a ring of mass m, radius r, and tilt θ is given, using Eq. (A16), by

$$\frac{\partial V_g}{\partial\theta}=\frac{m}{2\pi}\int\frac{\partial\nu(\eta)}{\partial\theta}[F_1'(\nu)-F_1'(\lambda)]d\eta. \tag{B3}$$

Far outside the core, from the equations analogous to Eqs. (A4)–(A6):

$$\lambda=r^2+O(1),\ \nu=a^2-(a^2-c^2)\cos^2\theta\sin^2\eta+O(r^{-2}), \tag{B4}$$

so that from Eq. (A16)

$$\frac{\partial\nu(\eta)}{\partial\theta}=(a^2-c^2)\sin^2\eta\sin 2\theta+O(r^{-2}). \tag{B5}$$

The function $f(\tau)$ decreases with τ, so at large distances $F_1'(\lambda)$ decreases like r^{-2} while $F_1'(\nu)$ tends to alimit which is independent of r; by Eq. (B5) the torque becomes a function of θ alone. If the oblateness c/a is not large, we can expand the expression for $f(\tau)$ for small values of $\sqrt{(\tau-c^2)/c^2}$; hence

$$F_1'(\nu)=\frac{2\pi G\rho_0 a^2}{3c^2}+O(r^{-2}) \tag{B6}$$

so that

$$\frac{\partial V_g}{\partial\theta}\to m\pi G\rho_0\frac{a^2(a^2-c^2)}{3c^2}\sin 2\theta=mA_1\cos\theta\sin\theta, \tag{B7}$$

where $A_1=2\pi G\rho_0 a^2(a^2-c^2)/3c^2$ is the coefficient in the definition (15). For other properties of this potential in the scale-free limit, see Sec. 5.1 of de Zeeuw & Pfenniger (1988).

REFERENCES

Arnaboldi, M., Barbaro, G., Buson, L., Capaccioli, M., & Longo, G. 1993b, A&A, 268, 103

Arnaboldi, M., Capaccioli, M., Cappellaro, E., Held, E. V., & Sparke, L. S. 1993a, A&A, 267, 21

Bertola, F. 1987, in The Structure and Dynamics of Elliptical Galaxies, IAU Symposium 127, edited by P. T. de Zeeuw (Reidel, Dordrecht)

Binney, J., & Tremaine, S. 1987, Galactic Dynamics (Princeton University Press, Princeton)

Carlson, B. C. 1979, Num. Math., 33, 1

Chandrasekhar, S. 1969, Ellipsoidal Figures of Equilibrium (Yale University Press, New Haven)

Christodoulou, D. M., Katz, N., Rix, H.-W., & Habe, A. 1992, ApJ, 395, 113

de Zeeuw, T. 1985, MNRAS, 216, 273

de Zeeuw, T., & Pfenniger, D. 1988, MNRAS, 235, 949; erratum MNRAS, 262, 1087

Goldreich, P. 1966, Rev. Geophys., 4, 411

Goldstein, H. 1980, Classical Mechanics, 2nd ed. (Addison-Wesley, Reading)

Heisler, J., Merritt, D., & Schwarzschild, M. 1982, ApJ, 258, 490

Katz, N., & Rix, H.-W. 1992, ApJ, 389, L55

Lichtenberg, A. J., & Lieberman, M. A. 1983, Regular and Stochastic Motion (Springer, New York)

Magnenat, P. 1982, A&A, 108, 89

Mould, J., Balick, B., Bothun, G., & Aaronson, M. 1982, ApJ, 260, L37

Mulder, W. A., & Hooimeyer, J. R. M. 1984, A&A, 134, 158

Press, W. H., Teukolsky, S. A., Vetterling, W., & Flammery, B. P. 1992, Numerical Recipes, 2nd ed. (Cambridge University Press, Cambridge)

Sackett, P. D., & Sparke, L. S. 1990, ApJ, 361, 408

Schechter, P. L., & Gunn, J. E. 1978, AJ, 83, 1360

Schechter, P. L., Sancisi, R., van Woerden, H., & Lynds, C. R. 1984, MNRAS, 208, 111

Schwarzschild, M. 1982, ApJ, 263, 599

Schweizer, F., Whitmore, B. C., & Rubin, V. C. 1983, AJ, 88, 909 (SWR)

Sparke, L. S. 1986, MNRAS, 219, 657

Sparke, L. S., & Casertano, S. 1988, MNRAS, 234, 873

Steiman-Cameron, T. Y., & Durisen, R. H. 1984, ApJ, 276, 101

Steiman-Cameron, T. Y., & Durisen, R. H. 1988, ApJ, 325, 26

Tohline, J. E., & Durisen, R. H. 1982, ApJ, 257, 94

van Gorkom, J. H., Schechter, P. L., & Kristian, J. 1987, ApJ, 314, 457

Whitmore, B. C. 1991, in Warped Disks and Inclined Rings around Galaxies, edited by S. Casertano *et al.* (Cambridge University Press, Cambridge)

Whitmore, B. C., Lucas, R. A., McElroy, B. D., Steiman-Cameron, T. Y., Sackett, P. D., & Olling, R. P. 1990, AJ, 100, 1489 (PRC)

Whitmore, B. C., McElroy, B. D., & Schweizer, F. 1987a, ApJ, 314, 439 (WMS)

Whitmore, B. C., McElroy, B. D., & Schweizer, F. 1987b, in Structure and Dynamics of Elliptical Galaxies, IAU Symposium No. 127, edited by P. T. de Zeeuw (Reidel, Dordrecht)